Geophysical Research Letters

RESEARCH LETTER
10.1002/2018GL077062

Key Points:
- A new stochastic aerosol-snow albedo model is developed to resolve aerosol size distribution internally mixed in various snow grains
- BC-induced snow single-scattering coalbedo enhancement and albedo reduction significantly decrease with increasing BC effective radii
- Polydisperse BC leads to smaller single-scattering coalbedo enhancement and albedo reduction than monodisperse BC with same effective radii

Supporting Information:
- Supporting Information S1
- Data Set S1

Correspondence to:
C. He,
cenlinhe@ucar.edu

Citation:
He, C., Liou, K.-N., & Takano, Y. (2018). Resolving size distribution of black carbon internally mixed with snow: Impact on snow optical properties and albedo. *Geophysical Research Letters*, *45*, 2697–2705. https://doi.org/10.1002/2018GL077062

Received 6 JAN 2018
Accepted 9 MAR 2018
Accepted article online 14 MAR 2018
Published online 25 MAR 2018

Resolving Size Distribution of Black Carbon Internally Mixed With Snow: Impact on Snow Optical Properties and Albedo

Cenlin He[1,2], Kuo-Nan Liou[2], and Yoshi Takano[2]

[1]Advanced Study Program, National Center for Atmospheric Research, Boulder, CO, USA, [2]Joint Institute for Regional Earth System Science and Engineering and Department of Atmospheric and Oceanic Sciences, University of California, Los Angeles, CA, USA

Abstract We develop a stochastic aerosol-snow albedo model that explicitly resolves size distribution of aerosols internally mixed with various snow grains. We use the model to quantify black carbon (BC) size effects on snow albedo and optical properties for BC-snow internal mixing. Results show that BC-induced snow single-scattering coalbedo enhancement and albedo reduction decrease by a factor of 2–3 with increasing BC effective radii from 0.05 to 0.25 μm, while polydisperse BC results in up to 40% smaller visible single-scattering coalbedo enhancement and albedo reduction compared to monodisperse BC with equivalent effective radii. We further develop parameterizations for BC size effects for application to climate models. Compared with a realistic polydisperse assumption and observed shifts to larger BC sizes in snow, respectively, assuming monodisperse BC and typical atmospheric BC effective radii could lead to overestimates of ~24% and ~40% in BC-snow albedo forcing averaged over different BC and snow conditions.

Plain Language Summary Snow albedo is a key element in the Earth and climate system, which is regulated by snow and impurity properties. Snow albedo can be substantially reduced by the presence of light-absorbing aerosols, such as black carbon (BC). However, very little attention has been paid to the impact of BC size on snow albedo reduction, while observations have shown large variations in BC size distribution in the atmosphere and snow. In this study, we have developed a new aerosol-snow albedo model to resolve aerosol size distribution mixed within various snow grains. We find that the BC effects on snow albedo decrease with increasing BC effective sizes and are also influenced by different assumptions of BC size distributions. We further develop parameterizations for BC size effects for application to climate models. This study points toward an urgent need for not only better model characterizations but also extensive measurements of BC size distribution in snow.

1. Introduction

Light-absorbing aerosols significantly reduce snow albedo after deposition onto snowpack (e.g., Flanner et al., 2007; Lee et al., 2017; Zhao et al., 2014), which further alters surface energy balance and hydrological cycle and hence regional climate (Menon et al., 2010; Qian et al., 2015). Black carbon (BC), the most important light-absorbing aerosol (Bond et al., 2013), has been observed as a strong driver to accelerated glacier retreat and snowmelt over high mountains (Di Mauro et al., 2017; Painter et al., 2013), midlatitude seasonal snowpack (Sterle et al., 2013; Wang et al., 2017), and polar regions (McConnell et al., 2007; Pedersen et al., 2015). The impacts of BC on snow albedo can be affected by a number of factors, including BC content in snow, BC and snow particle properties, and environmental conditions (e.g., He et al., 2014; He, Takano, & Liou, 2017; Kokhanovsky, 2013; Räisänen et al., 2017; Warren & Wiscombe, 1980). Thus, accurate predictions of BC effects on snow albedo and regional climate require comprehensive understanding and quantification that integrates these key factors.

Many modeling efforts have been made to investigate the effects of snow depth, density, grain size, BC concentration, and environmental variables (e.g., solar zenith angle and cloud cover) on snow albedo and its reduction by BC contamination (e.g., Aoki et al., 2011; Gardner & Sharp, 2010; Warren, 1982). These studies have assumed BC particles externally mixed with spherical snow grains in albedo modeling. However, snow grains tend to be nonspherical in reality (Dominé et al., 2003). Recent studies (Dang et al., 2016; Tuzet et al., 2017; Wang et al., 2017) further accounted for snow grain nonsphericity in BC-snow external mixing and showed smaller BC-induced albedo reductions for nonspherical snow grains than their spherical

counterparts. Moreover, Flanner et al. (2012) found that 32–73% of BC particles in global surface snow are internally mixed with snow, which enhances BC-induced snow albedo forcing by up to 86% compared with purely external mixing for snow spheres. Liou et al. (2014) and He et al. (2018) further combined the impact of BC-snow internal mixing and snow grain shapes and showed that the enhanced BC-induced snow albedo reduction by internal mixing could be offset by snow nonsphericity effect.

However, very little attention has been paid to the impact of BC size on snow albedo reduction, while observations have shown large variations in BC size distribution in the atmosphere and snow (Schwarz et al., 2013). Assuming lognormal BC size distributions in external mixing of BC and snow spheres, Dang et al. (2015) found smaller BC mass absorption cross sections for larger BC effective radii (area-weighted mean radii) from 0.05 to 0.15 μm. Assuming BC internally mixed with snow spheres, Flanner et al. (2012) also showed decreasing BC effective mass absorption cross sections with increasing BC effective radii from 0.05 to 0.5 μm. They further indicated noticeably weaker BC absorption in snow for lognormal BC size distributions compared with monodisperse BC with equivalent effective radii. Therefore, resolving BC size distribution and its impact could be critical to accurate estimates of BC-induced snow albedo reduction.

This study for the first time develops a novel aerosol-snow albedo model that explicitly resolves size distribution of aerosols internally mixed with various shapes of snow grains by extending our previous work (Liou et al., 2014; He, Takano, Liou, Yang, et al., 2017; He et al., 2018). We use the model to quantify BC size effects on snow albedo and single-scattering properties. We further develop parameterizations for BC size effects for application to climate models and show climatic implications for BC-snow albedo forcing.

2. Methods

2.1. A Stochastic Aerosol-Snow Albedo Model

Liou et al. (2014) have developed a multilayer Stochastic Aerosol-Snow Albedo Model (SASAM) that simulates multiple monodisperse aerosols internally/externally mixed with different shapes of snow grains. In the present study, we extend the SASAM model to explicitly resolve aerosol size distribution in aerosol-snow internal mixing. Specifically, we generate aerosols by random sampling from their size distributions (see the supporting information for details) and distribute them randomly within snow grains following a stochastic procedure (Liou et al., 2014) in order to represent the stochastic nature of atmospheric processes that form BC-snow mixtures (Flanner et al., 2012). Different snow grain structures are constructed in a 3-D coordinate system. We further compute spectral single-scattering properties (i.e., extinction efficiency [Q_e], single-scattering albedo [ω], and asymmetry factor [g]) of aerosol-snow mixtures using the geometric-optics surface wave (GOS) approach, described in details by Liou and Yang (2016). The GOS method can deal with complex particle structures with a wide size range and a high computational efficiency, which has been comprehensively validated with other particle-optic methods and laboratory measurements (He et al., 2015, 2016; Liou et al., 2011; Takano et al., 2013). Using the spectral single-scattering properties computed by GOS, we calculate spectral snow albedo based on the adding/doubling radiative transfer scheme (Takano & Liou, 1989). The SASAM model can be applied to various types of aerosols, including BC and dust. The number of snow layers in the SASAM model can be adjusted according to research goals. Snow aging processes are not accounted for in the current model.

2.2. Theoretical Calculations

In this study, we account for three types of snow grains, including sphere, spheroid, and Koch snowflake (Figure S1), with volume-equivalent sphere radii (R_v) of 100, 500, and 1,000 μm. These shapes are typical examples representing major structural characteristics of observed snow grains (Dominé et al., 2003). For comparison, we assume both monodisperse (constant radii) and polydisperse (lognormal) BC spheres internally mixed with snow, with BC effective radii (R_{BC}; area-weighted mean radii) of 0.05, 0.10, 0.15, 0.20, and 0.25 μm within the observed size range (Schwarz et al., 2013). Following Dentener et al. (2006) and Flanner et al. (2012), we use a geometric standard deviation of 1.8 for lognormal BC number size distributions. As such, the resulting geometric mean radii are 0.021, 0.042, 0.063, 0.084, and 0.105 μm, corresponding to the aforementioned effective radii, respectively. We assume BC mass concentrations (C_{BC}) of 10, 100, and 1,000 ppb (i.e., ng g^{-1}) in snow to represent slight, moderate, and severe BC contamination (Qian et al., 2015). We use BC and ice densities of 1.7 (Bond & Bergstrom, 2006) and 0.917 g cm^{-3} (Warren &

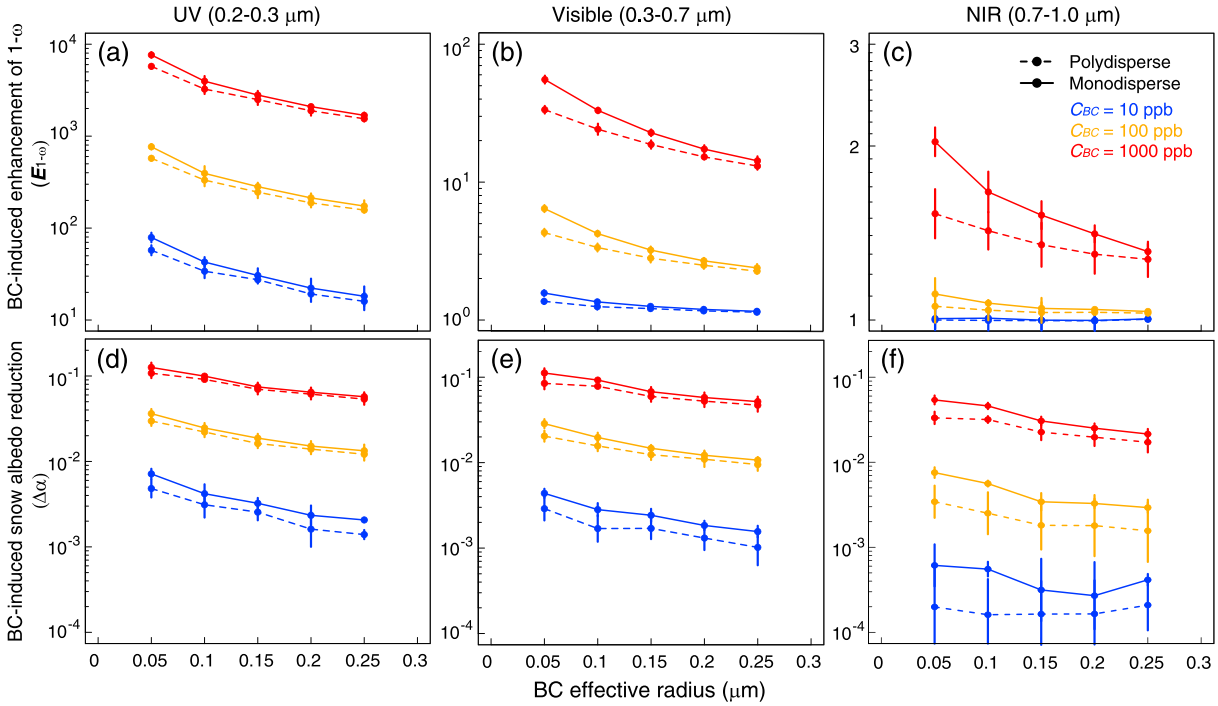

Figure 1. (a–c) Enhancement ($E_{1\text{-}\omega}$) of broadband snow single scattering coalbedo (1-ω) caused by black carbon (BC) concentrations (C_{BC}) of 10 (blue), 100 (orange), and 1,000 (red) ppb in snow as a function of BC effective radii by assuming polydisperse (dashed lines) and monodisperse (solid lines) BC inside snow grains at ultraviolet (UV, left column), visible (middle column), and near-infrared (NIR, right column) bands. The dots and vertical lines, respectively, are mean values and 95% uncertainty ranges by accounting for different snow shapes (i.e., spheres, spheroids, and Koch snowflakes) and volume-equivalent sphere radii (i.e., 100, 500, and 1,000 μm). (d–f) Same as the (a–c) but for BC-induced broadband snow albedo reduction ($\Delta\alpha$) with mean values (dots) and uncertainty range (1σ; vertical lines) by assuming different snow shapes (i.e., spheres, spheroids, and Koch snowflakes) with a volume-equivalent sphere radius of 100 μm. See Figure S4 for snow albedo reductions with volume-equivalent sphere radii of 500 and 1,000 μm. Note that uncertainties associated with some points in (a)–(f) are rather small.

Wiscombe, 1980), respectively. As a result, the number of BC inside each snow grain can be computed based on BC and snow particle sizes and densities as well as BC mass concentration. Spectral refractive indices of BC and snow are from Krekov (1993) and Warren and Brandt (2008), respectively.

We use the SASAM model (see section 2.1) to compute spectral optical properties and albedo of clean and BC-contaminated snow for wavelengths of 0.2–1.0 μm with a 0.01 μm interval, since BC in snow has rather small effects at wavelengths >1.0 μm (He, Takano, Liou, Yang, et al., 2017; He et al., 2018). We assume a homogeneous semiinfinite snowpack with an optical depth of 960 to obtain observed pure snow albedo following He et al. (2014), and a black underlying ground surface. We use a solar zenith angle of 49.5° with a cosine value of 0.65, which represents the insolation-weighted mean value for sunlit Earth hemisphere and the effective value for diffuse radiation under clouds (Dang et al., 2015). Broadband snow optical properties and albedo are further computed at ultraviolet (UV, 0.2–0.3 μm), visible (0.3–0.7 μm), and near-infrared (NIR, 0.7–1.0 μm) bands by integrating spectral values weighted by the incoming solar irradiance from the American Society for Testing and Materials reference data set (available at http://rredc.nrel.gov/solar/spectra/am1.5/; see also He, Takano, Liou, Yang, et al., 2017 for details). We note that negligible solar radiation reaches the surface at the UV band.

3. Results and Discussions

3.1. Impact on Snow Single-Scattering Properties

We do not discuss snow extinction efficiency and asymmetry factor in this study, because of negligible BC effects on these two properties (Figures S2 and S3), whereas BC significantly enhances snow single-scattering coalbedo (He, Takano, Liou, Yang, et al., 2017). Thus, we focus on BC size effects on snow single-scattering coalbedo. Figures 1a–1c show the BC-induced enhancement ($E_{1\text{-}\omega}$) in snow single-scattering coalbedo (1-ω) as a function of BC effective radii (R_{BC}) for monodisperse and polydisperse BC with different

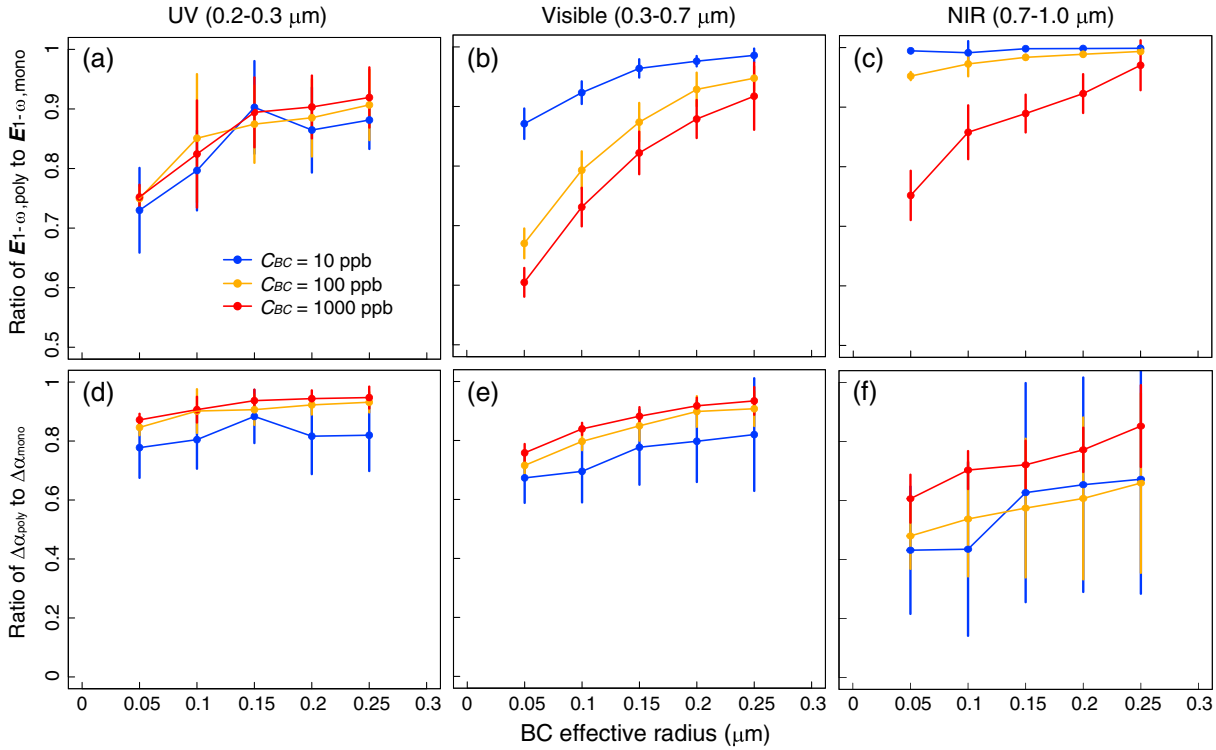

Figure 2. (a–c) Ratios of black carbon (BC)-induced enhancement ($E_{1\text{-}\omega}$) in broadband snow single-scattering coalbedo (1-ω) with polydisperse BC ($E_{1\text{-}\omega,\text{poly}}$) to that with monodisperse BC ($E_{1\text{-}\omega,\text{mono}}$) as a function of BC effective radii (R_{BC}) for BC concentrations (C_{BC}) of 10 (blue), 100 (orange), and 1,000 (red) ppb in snow at ultraviolet (UV, left column), visible (middle column), and near-infrared (NIR, right column) bands. The dots and vertical lines, respectively, are mean values and uncertainty ranges (1σ) by accounting for different snow shapes (i.e., spheres, spheroids, and Koch snowflakes) and volume-equivalent sphere radii (i.e., 100, 500, and 1,000 μm). (d–f) Same as the (a–c) but for ratios of BC-induced broadband snow albedo reduction ($\Delta\alpha$) with polydisperse BC ($\Delta\alpha_{\text{poly}}$) to that with monodisperse BC ($\Delta\alpha_{\text{mono}}$).

concentrations in snow. Here $E_{1\text{-}\omega}$ is defined as the ratio of single-scattering coalbedo for BC-contaminated snow to that for pure snow. The results show that snow grain shapes and sizes have rather small impacts on $E_{1\text{-}\omega}$ (1σ variation $<$5%), consistent with previous studies (He, Takano, Liou, Yang, et al., 2017). The $E_{1\text{-}\omega}$, depending on R_{BC}, are 15–55 and 2.5–6 at the visible band for 1,000 and 100 ppb BC in snow, respectively, which are about 1 order of magnitude higher than those at the NIR band. We find decreasing $E_{1\text{-}\omega}$ with increasing R_{BC} in all cases (Figures 1a–1c). The decreases are stronger for higher BC concentrations, with a 50–60% (60–75%) lower visible $E_{1\text{-}\omega}$ for a R_{BC} of 0.25 μm than that for a R_{BC} of 0.05 μm with 100 (1,000) ppb BC in snow. This agrees with the conclusion in Flanner et al. (2012), which showed that BC absorption in snow decreases as R_{BC} increases from 0.05 to 0.5 μm.

Furthermore, we find that $E_{1\text{-}\omega}$ for polydisperse BC is consistently lower than that for monodisperse BC regardless of BC effective radii, concentrations, snow grain sizes, and shapes (Figures 1a–1c). The relative differences in $E_{1\text{-}\omega}$ between polydisperse and monodisperse BC increase as R_{BC} decreases or BC concentration increases (Figures 2b and 2c), with a stronger dependence on R_{BC} for higher BC concentrations, except for the UV band (Figure 2a). For 1,000 ppb BC in snow, polydisperse BC shows lower visible $E_{1\text{-}\omega}$ than monodisperse BC by ~40% and ~10% with R_{BC} of 0.05 and 0.25 μm, respectively, while the relative differences are ~13% and ~2% for 10 ppb BC (Figures 2a–2c). Compared with the visible band, the differences in $E_{1\text{-}\omega}$ at the NIR band between polydisperse and monodisperse BC are much smaller (Figure 2c). Flanner et al. (2012) also found smaller BC absorption in snow for polydisperse BC relative to that for monodisperse BC, with larger differences for smaller R_{BC}.

3.2. Impact on Snow Albedo

Snow albedo is significantly affected by snow grain size, grain shape, and BC concentration, which has been discussed in details by previous studies (e.g., He et al., 2018; Warren & Wiscombe, 1980). Here we focus on BC

size effects on BC-induced snow albedo reduction. Figures 1d–1f show the BC-induced snow albedo reduction ($\Delta\alpha$) as a function of R_{BC} for monodisperse and polydisperse BC with different concentrations in fresh snow (R_v = 100 μm). The results indicate that $\Delta\alpha$ decreases substantially with increasing R_{BC} in all cases, with a factor of 2–3 decrease in $\Delta\alpha$ for an increasing R_{BC} from 0.05 to 0.25 μm. For example, the visible $\Delta\alpha$ are ~0.1 and ~0.0035 for 1,000 and 10 ppb BC in snow, respectively, with a R_{BC} of 0.05 μm, which reduce to ~0.05 and ~0.0012 for a R_{BC} of 0.25 μm. Similar strong decreases in $\Delta\alpha$ with R_{BC} also occur at the UV and NIR bands, except for 10 ppb BC at the NIR band (Figure 1f). We find that the sensitivity of $\Delta\alpha$ to snow grain shapes (i.e., relative change in $\Delta\alpha$ caused by different shapes) is weak for high BC concentrations (≥100 ppb) at the UV and visible bands (Figures 1d and 1e) but becomes important for small BC concentrations (10 ppb) particularly at the NIR band (Figure 1f). However, the values of $\Delta\alpha$ at the NIR band are a factor of 2–25 smaller than those at the UV and visible bands. These features of $\Delta\alpha$ have also been found for aged snow with R_v of 500 and 1,000 μm (Figure S4).

Moreover, similar to $E_{1\text{-}\omega}$, we find that $\Delta\alpha$ for polydisperse BC is consistently lower than that for monodisperse BC under different BC effective radii, concentrations, snow grain sizes, and shapes. Figures 2d–2f show that the relative differences in $\Delta\alpha$ between polydisperse and monodisperse BC decrease as the R_{BC} increases, with differences of 30% and 10% for R_{BC} of 0.05 and 0.25 μm at the visible band, respectively, for 100 ppb BC in snow. Contrary to $E_{1\text{-}\omega}$, the relative differences in $\Delta\alpha$ between polydisperse and monodisperse BC are larger for lower BC concentrations. For example, the relative differences for 10 ppb BC at the visible band are a factor of 1.3–2.8 larger than those for 1,000 ppb BC (Figure 2e). In addition, the results indicate larger relative differences in $\Delta\alpha$ between polydisperse and monodisperse BC at the NIR band than those at the visible and UV bands, though much smaller values of $\Delta\alpha$ at the NIR band. We further note that the relative differences are sensitive to snow grain sizes and shapes for small BC concentrations (10 ppb) and all cases at the NIR band (Figure 2f), which are dominated by snow shape effects (Figures S5 and S6).

3.3. Parameterizations for BC Size Effects

For application to land surface and climate models, we further develop parameterizations to account for BC size effects on snow single-scattering coalbedo enhancement ($E_{1\text{-}\omega}$) and albedo reduction ($\Delta\alpha$) caused by BC-snow internal mixing. Figure 3 summarizes the $E_{1\text{-}\omega}$ and $\Delta\alpha$ of polydisperse BC with different R_{BC} as a function of those with a R_{BC} of 0.05 μm for various snow grain sizes, grain shapes, and BC concentrations. We find that the $E_{1\text{-}\omega}$ and $\Delta\alpha$ for a certain R_{BC} ($E_{1\text{-}\omega,RBC}$ and $\Delta\alpha_{RBC}$) have good quantitative relationships with those for a R_{BC} of 0.05 μm ($E_{1\text{-}\omega,RBC\,=\,0.05}$ and $\Delta\alpha_{RBC\,=\,0.05}$), respectively, as follows:

$$E_{1-\omega,R_{BC}} = d_{\lambda,R_{BC}} \times E_{1-\omega,R_{BC}=0.05}^{f_{\lambda,R_{BC}}} \tag{1a}$$

with

$$d_{\lambda,R_{BC}} = \left(\frac{R_{BC}}{0.05}\right)^{m_\lambda}, f_{\lambda,R_{BC}} = \left(\frac{R_{BC}}{0.05}\right)^{n_\lambda} \tag{1b}$$

$$\Delta\alpha_{R_{BC}} = k_{\lambda,R_{BC}} \times \Delta\alpha_{R_{BC}=0.05} \tag{2a}$$

with

$$k_{\lambda,R_{BC}} = \left(\frac{R_{BC}}{0.05}\right)^{p_\lambda} \tag{2b}$$

where $d_{\lambda,R_{BC}}$, $f_{\lambda,R_{BC}}$, and $k_{\lambda,R_{BC}}$ are empirical coefficients depending on wavelength (λ) and BC effective radii (R_{BC}). The m_λ, n_λ, and p_λ are derived from nonlinear regression processes with R^2 of >0.96 and normalized mean biases of −2.5%–2% (Figure 3). Here the results for the case of R_{BC} = 0.05 μm ($E_{1\text{-}\omega,RBC\,=\,0.05}$ and $\Delta\alpha_{RBC\,=\,0.05}$) are used as reference values in the parameterization. The coefficients (m_λ, n_λ, and p_λ; see Table S1) represent the mean impact of R_{BC} on $E_{1\text{-}\omega}$ and $\Delta\alpha$ under different BC and snow conditions (i.e., BC concentration, snow grain size, and shape). Similar relationships have also been found for monodisperse BC (see Figure S7 and Table S1).

In addition, we also summarize the $E_{1\text{-}\omega}$ and $\Delta\alpha$ for polydisperse BC as a function of those for monodisperse BC in all cases, as illustrated in Figure 4. Interestingly, $\Delta\alpha$ and the logarithm of $E_{1\text{-}\omega}$ for polydisperse BC show good linear relationships with those for monodisperse BC, respectively. Thus, we quantitatively relate the $E_{1\text{-}\omega}$

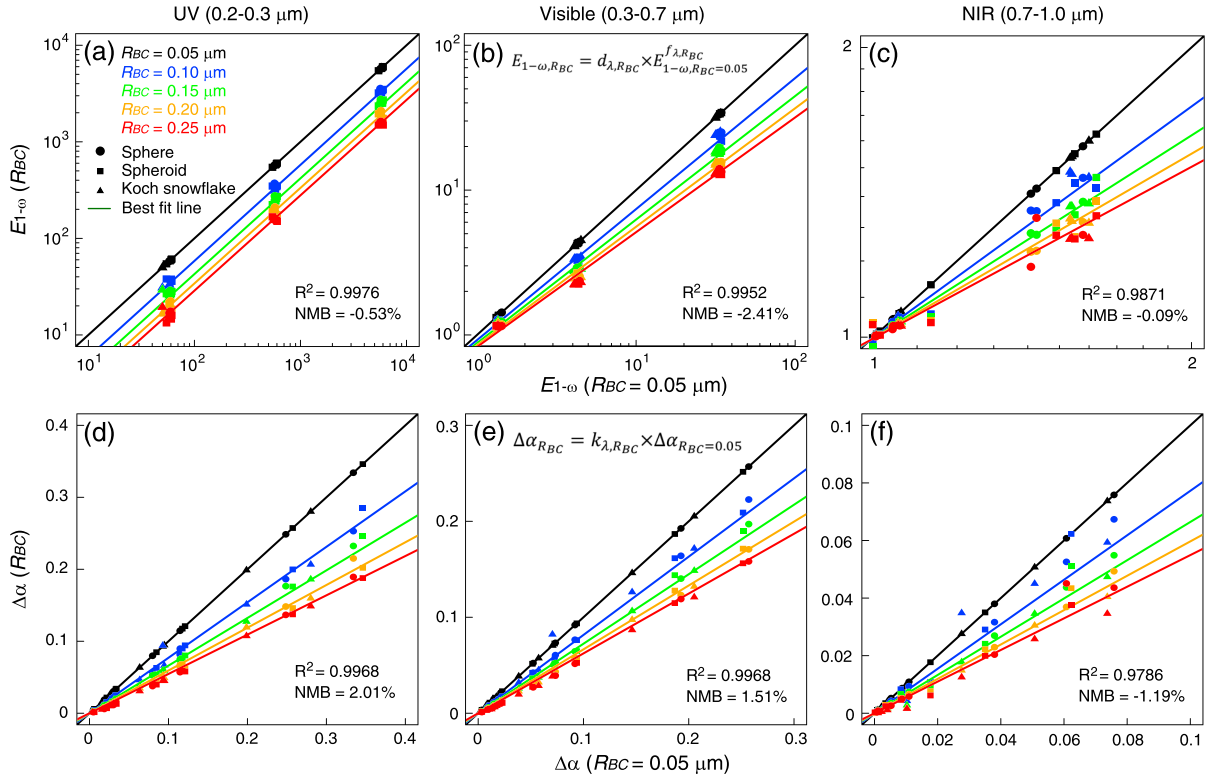

Figure 3. (a–c) Black carbon (BC)-induced enhancement ($E_{1\text{-}\omega}$) in broadband snow single scattering coalbedo (1-ω) for polydisperse BC with effective radii (R_{BC}) of 0.05 (black), 0.1 (blue), 0.15 (green), 0.2 (orange), and 0.25 (red) μm ($E_{1\text{-}\omega,RBC}$) as a function of that with an effective radius of 0.05 μm ($E_{1\text{-}\omega,RBC\ =\ 0.05}$) at ultraviolet (UV, left column), visible (middle column), and near-infrared (NIR, right column) bands by accounting for snow spheres (circles), spheroids (squares), and Koch snowflakes (triangles) with volume-equivalent sphere radii of 100, 500, and 1,000 μm for BC concentrations of 10, 100, and 1,000 ppb in snow. (d–f): Same as the (a–c) but for BC-induced broadband snow albedo reduction ($\Delta\alpha$). Also shown are best fitting lines (solid), total R^2 and normalized mean biases (NMB), and parameterization equations (equations (1a) and (1b) and (2a) and (2b); see Table S1 for coefficient values). Note that *x* axis and *y* axis in (a–c) have logarithmic scales.

and $\Delta\alpha$ for polydisperse BC ($E_{1\text{-}\omega,\text{poly}}$ and $\Delta\alpha_{\text{poly}}$) to those for monodisperse BC ($E_{1\text{-}\omega,\text{mono}}$ and $\Delta\alpha_{\text{mono}}$), respectively, as follows:

$$E_{1-\omega,\text{poly}} = a_\lambda \times E_{1-\omega,\text{mono}}^{b_\lambda} \quad (3)$$

$$\Delta\alpha_{\text{poly}} = c_\lambda \times \Delta\alpha_{\text{mono}} \quad (4)$$

where a_λ, b_λ, and c_λ are empirical wavelength-dependent coefficients derived from linear regression processes, with R^2 of ≥0.95 and normalized mean biases of −1%–2% (Figure 4). The coefficients (a_λ, b_λ, and c_λ; see Table S1) represent the mean effects of accounting for BC polydisperse size distribution in BC-snow internal mixing compared with monodisperse size distribution under different BC and snow conditions.

The present parameterizations (equations (1a) and (1b), (2a) and (2b), (3), and (4)), as first-order approximations, can be used to adjust $E_{1\text{-}\omega}$ and $\Delta\alpha$ depending on either R_{BC} or polydisperse/monodisperse size distribution with a high accuracy. We note that these relationships should be used with caution when applying to extremely small ($R_{BC} < 0.05$ μm) or large ($R_{BC} > 0.25$ μm) BC particles.

4. Climatic Implications

The aforementioned analysis highlights the critical role of BC particle size in determining BC-induced snow albedo reduction. Previous studies often assumed R_{BC} of 0.05–0.1 μm (typical values for BC in the atmosphere) in snow albedo modeling (e.g., Dang et al., 2015; Flanner et al., 2007; He et al., 2018; Warren & Wiscombe, 1980). However, recent observations (Schwarz et al., 2013) have shown that a significant portion of BC particles in snow can shift to larger sizes (radii >0.25 μm), which are much larger than those typically seen in the atmosphere. Based on the present parameterization (equations (2a) and (2b)), we estimate that

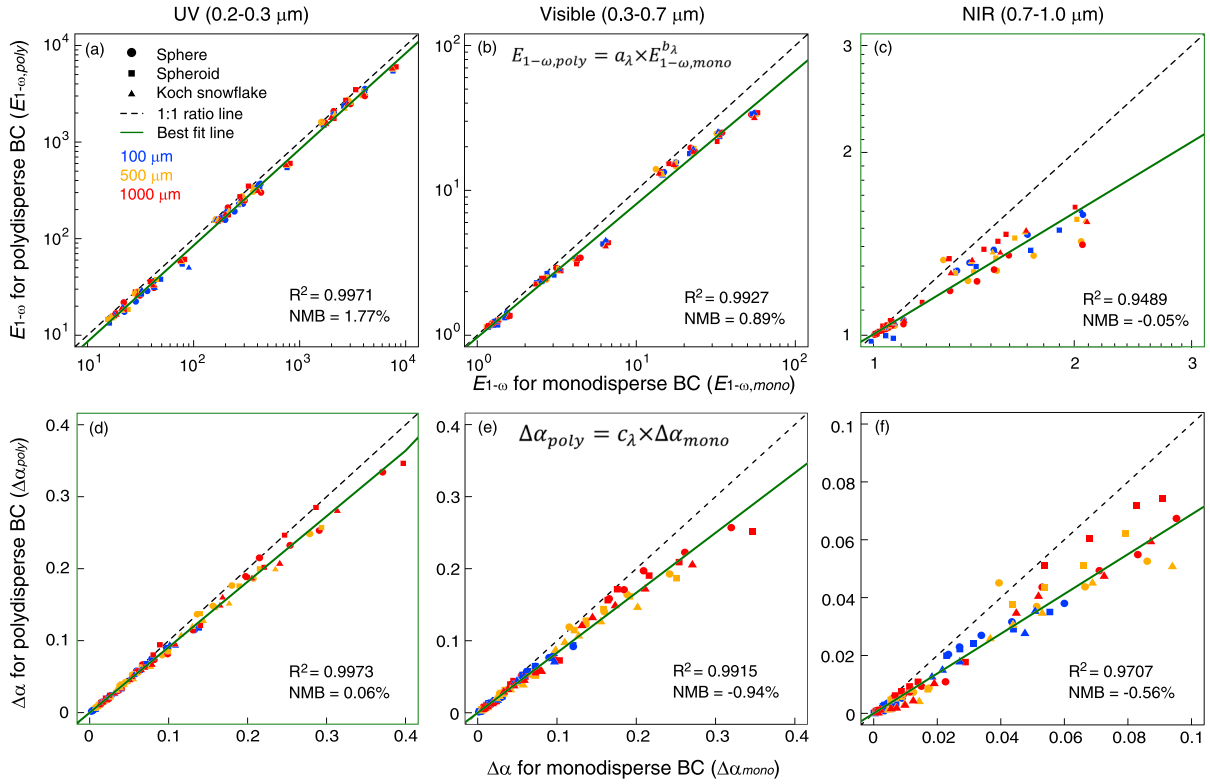

Figure 4. (a–c) Black carbon (BC)-induced enhancement ($E_{1\text{-}\omega}$) in broadband snow single scattering coalbedo (1-ω) for polydisperse BC ($E_{1\text{-}\omega,\text{poly}}$) as a function of that for monodisperse BC ($E_{1\text{-}\omega,\text{mono}}$) at ultra-violet (UV, left column), visible (middle column), and near-infrared (NIR, right column) bands by accounting for snow spheres (circles), spheroids (squares), and Koch snowflakes (triangles) with volume-equivalent sphere radii of 100 (blue), 500 (orange), and 1,000 (red) μm for BC concentrations of 10, 100, and 1,000 ppb with BC effective radii of 0.05, 0.1, 0.15, 0.2, and 0.25 μm. (d–f) Same as the (a–c) but for BC-induced broadband snow albedo reduction ($\Delta\alpha$). Also shown are 1:1 ratio lines (black dashed), best fitting lines (dark green solid), total R^2 and normalized mean biases (NMB), and parameterization equations (equations (3) and (4); see Table S1 for coefficient values). Note that *x* axis and *y* axis in (a–c) have logarithmic scales.

BC-induced snow albedo reduction can be decreased by about 38% and 45% (relative differences) at the visible and NIR bands, respectively, averaged over different BC concentrations and snow grain sizes and shapes, when increasing R_{BC} from 0.05 to 0.25 μm for polydisperse BC. For example, as R_{BC} increases from 0.05 to 0.25 μm, the snow albedo reduction (integrated through the solar spectrum) decreases by 0.006 and 0.032 (absolute values) for 100 ppb BC in fresh (R_v = 100 μm) and aged (R_v = 1,000 μm) snow, respectively, averaged over different snow grain shapes. This leads to reductions of about 1.2 (0.54) and 6.4 (2.9) W m^{-2} in springtime BC-snow albedo radiative forcing for fresh and aged snow, respectively, over the northern midlatitude (Arctic) snowpack, where the monthly all-sky downward surface solar radiation is ~200 (~90) W m^{-2} in spring (Dang et al., 2017). This suggests that previous modeling studies using typical atmospheric BC sizes ($R_{BC} \leq 0.1$ μm) have likely overestimated BC contamination effects on snow albedo, and the observed shift to larger BC sizes in snow could averagely reduce BC-snow albedo forcing by ~40% or more for BC-snow internal mixing under different BC and snow conditions.

Moreover, we find that assuming monodisperse BC, instead of polydisperse BC, overestimates BC-induced snow albedo reduction by about 17% (32%) at the visible (NIR) band, averaged over different BC concentrations, effective radii, snow grain sizes, and shapes, based on the present parameterization (equation (4)). This leads to a mean overestimate of ~24% in BC-snow albedo forcing for BC-snow internal mixing caused by the monodisperse assumption. For example, the BC-induced albedo reductions (integrated through the solar spectrum) increase by up to 0.006 and 0.018 (absolute values) for 100 ppb BC in fresh and aged snow averaged over different snow grain shapes, respectively, when assuming monodisperse BC instead of polydisperse BC. This results in increases of up to 1.2 (0.54) and 3.6 (1.6) W m^{-2} in springtime BC-snow albedo forcing for 100 ppb BC in fresh and aged snow, respectively, over the northern midlatitude (Arctic) snowpack. Thus, it is necessary to explicitly account for polydisperse BC size distribution in BC-snow internal mixtures.

We note that the BC size effects are comparable to the impacts of snow grain shape (spherical versus nonspherical) and BC-snow mixing state (internal versus external) on BC-induced snow albedo reduction (He et al., 2018). This points toward an urgent need for not only better model characterizations but also extensive measurements of BC size distribution in snow, since rather limited observations are currently available.

5. Conclusions

We have developed a novel SASAM that explicitly resolves size distribution of aerosols internally mixed with various shapes of snow grains. We used this model to quantify BC size effects on snow optical properties and albedo for BC-snow internal mixing. We found that BC-induced snow single-scattering coalbedo enhancement and albedo reduction decrease by a factor of 2–3 as BC effective radii increase from 0.05 to 0.25 μm. Compared with monodisperse BC, polydisperse BC with equivalent effective radii leads to consistently lower BC-induced snow single-scattering coalbedo enhancement and albedo reduction in all cases (e.g., by up to 40% at the visible band), with the relative differences increase as BC effective radii decrease. Moreover, the BC size effects are insensitive to snow grain shape and size for BC-induced snow single-scattering coalbedo enhancement, but are more sensitive for BC-induced snow albedo reduction with small BC concentrations and at the NIR band.

For application to land surface and climate models, we further developed parameterizations to account for BC size effects on snow albedo and single-scattering coalbedo. We found that the observed shift to larger BC sizes in snow could averagely reduce BC-snow albedo forcing by ~40% or more for BC-snow internal mixing, while assuming monodisperse BC leads to an overestimate of ~24% in BC-snow albedo forcing averaged over different BC and snow conditions, compared with a more realistic polydisperse assumption. The results highlight the critical role of BC particle size in understanding BC-snow interactions and the necessity for more extensive measurements and better model characterizations of BC size distribution in snow.

In addition, the SASAM model and approach developed here are also applicable to other light-absorbing aerosols, including dust, which usually coexists with BC in snow (Skiles & Painter, 2017; Wang et al., 2017). The dust size effects on snow albedo, albeit expected to be qualitatively similar to BC size effects, require further quantifications. Moreover, modeling studies (e.g., Dang et al., 2017) have suggested that the presence of dust in snow could reduce the BC impact on albedo and hence may weaken BC size effects, which will be investigated in future work.

Acknowledgments
The authors thank the reviewers for their constructive comments. This study was supported by NSF grant AGS-1660587. The National Center for Atmospheric Research (NCAR) is sponsored by the National Science Foundation (NSF). C. He was supported by the NCAR Advanced Study Program (ASP) Fellowship sponsored by NSF. Users can access the new data produced in this study via the supporting information or the corresponding author without any restrictions. The authors declare no conflicts of interest.

References

Aoki, T., Kuchiki, K., Niwano, M., Kodama, Y., Hosaka, M., & Tanaka, T. (2011). Physically based snow albedo model for calculating broadband albedos and the solar heating profile in snowpack for general circulation models. *Journal of Geophysical Research*, *116*, D11114. https://doi.org/10.1029/2010JD015507

Bond, T. C., & Bergstrom, R. W. (2006). Light absorption by carbonaceous particles: An investigative review. *Aerosol Science and Technology*, *40*(1), 27–67. https://doi.org/10.1080/02786820500421521

Bond, T. C., Doherty, S. J., Fahey, D. W., Forster, P. M., Berntsen, T., DeAngelo, B. J., et al. (2013). Bounding the role of black carbon in the climate system: A scientific assessment. *Journal of Geophysical Research: Atmospheres*, *118*, 5380–5552. https://doi.org/10.1002/jgrd.50171

Dang, C., Brandt, R. E., & Warren, S. G. (2015). Parameterizations for narrowband and broadband albedo of pure snow and snow containing mineral dust and black carbon. *Journal of Geophysical Research: Atmospheres*, *120*, 5446–5468. https://doi.org/10.1002/2014JD022646

Dang, C., Fu, Q., & Warren, S. (2016). Effect of snow grain shape on snow albedo. *Journal of the Atmospheric Sciences*, *73*(9), 3573–3583. https://doi.org/10.1175/JAS-D-15-0276.1

Dang, C., Warren, S. G., Fu, Q., Doherty, S. J., Sturm, M., & Su, J. (2017). Measurements of light-absorbing particles in snow across the Arctic, North America, and China: Effects on surface albedo. *Journal of Geophysical Research: Atmospheres*, *122*, 10,149–10,168. https://doi.org/10.1002/2017JD027070

Dentener, F., Kinne, S., Bond, T., Boucher, O., Cofala, J., Generoso, S., et al. (2006). Emissions of primary aerosol and precursor gases in the years 2000 and 1750 prescribed data-sets for AeroCom. *Atmospheric Chemistry and Physics*, *6*(12), 4321–4344. https://doi.org/10.5194/acp-6-4321-2006

Di Mauro, B., Baccolo, G., Garzonio, R., Giardino, C., Massabò, D., Piazzalunga, A., et al. (2017). Impact of impurities and cryoconite on the optical properties of the Morteratsch Glacier (Swiss Alps). *The Cryosphere*, *11*(6), 2393–2409. https://doi.org/10.5194/tc-11-2393-2017

Dominé, F., Lauzier, T., Cabanes, A., Legagneux, L., Kuhs, W. F., Techmer, K., & Heinrichs, T. (2003). Snow metamorphism as revealed by scanning electron microscopy. *Microscopy Research and Technique*, *62*(1), 33–48. https://doi.org/10.1002/jemt.10384

Flanner, M. G., Liu, X., Zhou, C., Penner, J. E., & Jiao, C. (2012). Enhanced solar energy absorption by internally-mixed black carbon in snow grains. *Atmospheric Chemistry and Physics*, *12*(10), 4699–4721. https://doi.org/10.5194/acp-12-4699-2012

Flanner, M. G., Zender, C. S., Randerson, J. T., & Rasch, P. J. (2007). Present-day climate forcing and response from black carbon in snow. *Journal of Geophysical Research*, *112*, D11202. https://doi.org/10.1029/2006JD008003

Gardner, A. S., & Sharp, M. J. (2010). A review of snow and ice albedo and the development of a new physically based broadband albedo parameterization. *Journal of Geophysical Research*, *115*, F01009. https://doi.org/10.1029/2009JF001444

He, C., Li, Q., Liou, K.-N., Takano, Y., Gu, Y., Qi, L., et al. (2014). Black carbon radiative forcing over the Tibetan Plateau. *Geophysical Research Letters*, *41*, 7806–7813. https://doi.org/10.1002/2014GL062191

He, C., Liou, K. N., Takano, Y., Yang, P., Qi, L., & Chen, F. (2018). Impact of grain shape and multiple black carbon internal mixing on snow albedo: Parameterization and radiative effect analysis. *Journal of Geophysical Research: Atmospheres*, *123*, 1253–1268. https://doi.org/10.1002/2017JD027752

He, C., Liou, K. N., Takano, Y., Zhang, R., Levy Zamora, M., Yang, P., et al. (2015). Variation of the radiative properties during black carbon aging: Theoretical and experimental intercomparison. *Atmospheric Chemistry and Physics*, *15*(20), 11,967–11,980. https://doi.org/10.5194/acp-15-11967-2015

He, C., Takano, Y., & Liou, K.-N. (2017). Close packing effects on clean and dirty snow albedo and associated climatic implications. *Geophysical Research Letters*, *44*, 3719–3727. https://doi.org/10.1002/2017GL072916

He, C., Takano, Y., Liou, K. N., Yang, P., Li, Q., & Chen, F. (2017). Impact of snow grain shape and black carbon-snow internal mixing on snow optical properties: Parameterizations for climate models. *Journal of Climate*, *30*(24), 10,019–10,036. https://doi.org/10.1175/JCLI-D-17-0300.1

He, C., Takano, Y., Liou, K.-N., Yang, P., Li, Q., & Mackowski, D. W. (2016). Intercomparison of the GOS approach, superposition Tmatrix method, and laboratory measurements for black carbon optical properties during aging. *Journal of Quantitative Spectroscopy & Radiative Transfer*, *184*, 287–296. https://doi.org/10.1016/j.jqsrt.2016.08.004

Kokhanovsky, A. (2013). Spectral reflectance of solar light from dirty snow: A simple theoretical model and its validation. *The Cryosphere*, *7*(4), 1325–1331. https://doi.org/10.5194/tc-7-1325-2013

Krekov, G. M. (1993). Models of atmospheric aerosols. In S. G. Jennings (Ed.), *Aerosol Effects on Climate* (pp. 9–72). Tucson, AZ: University of Arizona Press.

Lee, W.-L., Liou, K. N., He, C., Liang, H.-C., Wang, T.-C., Li, Q., et al. (2017). Impact of absorbing aerosol deposition on snow albedo reduction over the southern Tibetan plateau based on satellite observations. *Theoretical and Applied Climatology*, *129*(3–4), 1373–1382. https://doi.org/10.1007/s00704-016-1860-4

Liou, K. N., Takano, Y., He, C., Yang, P., Leung, R. L., Gu, Y., & Lee, W. L. (2014). Stochastic parameterization for light absorption by internally mixed BC/dust in snow grains for application to climate models. *Journal of Geophysical Research: Atmospheres*, *119*, 7616–7632. https://doi.org/10.1002/2014JD021665

Liou, K. N., Takano, Y., & Yang, P. (2011). Light absorption and scattering by aggregates: Application to black carbon and snow grains. *Journal of Quantitative Spectroscopy & Radiative Transfer*, *112*(10), 1581–1594. https://doi.org/10.1016/j.jqsrt.2011.03.007

Liou, K. N., & Yang, P. (2016). *Light scattering by ice crystals: Fundamentals and applications* (pp. 168–173). Cambridge, UK: Cambridge University Press. https://doi.org/10.1017/CBO9781139030052

McConnell, J. R., Edwards, R., Kok, G. L., Flanner, M. G., Zender, C. S., Saltzman, E. S., et al. (2007). 20th-century industrial black carbon emissions altered arctic climate forcing. *Science*, *317*(5843), 1381–1384. https://doi.org/10.1126/science.1144856

Menon, S., Koch, D., Beig, G., Sahu, S., Fasullo, J., & Orlikowski, D. (2010). Black carbon aerosols and the third polar ice cap. *Atmospheric Chemistry and Physics*, *10*(10), 4559–4571. https://doi.org/10.5194/acp-10-4559-2010

Painter, T. H., Flanner, M. G., Kaser, G., Marzeion, B., VanCuren, R. A., & Abdalati, W. (2013). End of the Little Ice Age in the Alps forced by industrial black carbon. *Proceedings of the National Academy of Sciences of the United States of America*, *110*(38), 15,216–15,221. https://doi.org/10.1073/pnas.1302570110

Pedersen, C. A., Gallet, J.-C., Ström, J., Gerland, S., Hudson, S. R., Forsström, S., et al. (2015). In situ observations of black carbon in snow and the corresponding spectral surface albedo reduction. *Journal of Geophysical Research: Atmospheres*, *120*, 1476–1489. https://doi.org/10.1002/2014JD022407

Qian, Y., Yasunari, T. J., Doherty, S. J., Flanner, M. G., Lau, W. K. M., Ming, J., et al. (2015). Light-absorbing particles in snow and ice: Measurement and modeling of climatic and hydrological impact. *Advances in Atmospheric Sciences*, *32*(1), 64–91. https://doi.org/10.1007/s00376-014-0010-0

Räisänen, P., Makkonen, R., Kirkevåg, A., & Debernard, J. B. (2017). Effects of snow grain shape on climate simulations: Sensitivity tests with the Norwegian Earth System Model. *The Cryosphere*, *11*(6), 2919–2942. https://doi.org/10.5194/tc-11-2919-2017

Schwarz, J. P., Gao, R. S., Perring, A. E., Spackman, J. R., & Fahey, D. W. (2013). Black carbon aerosol size in snow. *Scientific Reports*, *3*(1), 1356. https://doi.org/10.1038/srep01356

Skiles, S. M., & Painter, T. H. (2017). Daily evolution in dust and black carbon content, snow grain size, and snow albedo during snowmelt, Rocky Mountains, Colorado. *Journal of Glaciology*, *63*(237), 118–132. https://doi.org/10.1017/jog.2016.125

Sterle, K. M., McConnell, J. R., Dozier, J., Edwards, R., & Flanner, M. G. (2013). Retention and radiative forcing of black carbon in eastern Sierra Nevada snow. *The Cryosphere*, *7*(1), 365–374. https://doi.org/10.5194/tc-7-365-2013

Takano, Y., & Liou, K. N. (1989). Solar radiative transfer in cirrus clouds. Part II. Theory and computation of multiple scattering in an anisotropic medium. *Journal of the Atmospheric Sciences*, *46*(1), 20–36. https://doi.org/10.1175/1520-0469(1989)046%3C0020:SRTICC%3E2.0.CO;2

Takano, Y., Liou, K. N., Kahnert, M., & Yang, P. (2013). The single-scattering properties of black carbon aggregates determined from the geometric-optics surface-wave approach and the T-matrix method. *Journal of Quantitative Spectroscopy & Radiative Transfer*, *125*, 51–56. https://doi.org/10.1016/j.jqsrt.2013.04.006

Tuzet, F., Dumont, M., Lafaysse, M., Picard, G., Arnaud, L., Voisin, D., et al. (2017). A multilayer physically based snowpack model simulating direct and indirect radiative impacts of light-absorbing impurities in snow. *The Cryosphere*, *11*(6), 2633–2653. https://doi.org/10.5194/tc-11-2633-2017

Wang, X., Pu, W., Ren, Y., Zhang, X., Zhang, X., Shi, J., et al. (2017). Observations and model simulations of snow albedo reduction in seasonal snow due to insoluble light-absorbing particles during 2014 Chinese survey. *Atmospheric Chemistry and Physics*, *17*(3), 2279–2296. https://doi.org/10.5194/acp-17-2279-2017

Warren, S. G. (1982). Optical properties of snow. *Reviews of Geophysics and Space Physics*, *20*(1), 67–89. https://doi.org/10.1029/RG020i001p00067

Warren, S. G., & Brandt, R. E. (2008). Optical constants of ice from the ultraviolet to the microwave: A revised compilation. *Journal of Geophysical Research*, *113*, D14220. https://doi.org/10.1029/2007JD009744

Warren, S. G., & Wiscombe, W. J. (1980). A model for the spectral albedo of snow. 2. Snow containing atmospheric aerosols. *Journal of the Atmospheric Sciences*, *37*(12), 2734–2745. https://doi.org/10.1175/1520-0469(1980)037%3C2734:AMFTSA%3E2.0.CO;2

Zhao, C., Hu, Z., Qian, Y., Ruby Leung, L., Huang, J., Huang, M., et al. (2014). Simulating black carbon and dust and their radiative forcing in seasonal snow: A case study over North China with field campaign measurements. *Atmospheric Chemistry and Physics*, *14*(20), 11,475–11,491. https://doi.org/10.5194/acp-14-11475-2014